

**PETROGENETIC AND SHOCK HISTORY OF MARE BASALTIC LUNAR METEORITE NORTHWEST AFRICA 4734.** J. Chen<sup>1,2</sup>, A. Wang<sup>2</sup>, B. L. Jolliff<sup>2</sup>, R. L. Korotev<sup>2</sup>, Z. C. Ling<sup>1, \*</sup>, X. H. Fu<sup>1</sup> and Y. H. Ni<sup>1</sup> <sup>1</sup>Institute of Space Sciences, Shandong University, Weihai, 264209, China (merchenj@mail.sdu.edu.cn, zcling@sdu.edu.cn), <sup>2</sup>Department of Earth & Planetary Sciences and McDonnell Center for the Space Sciences, Washington University in St. Louis, MO, 63130.

**Introduction:** In contrast to the many mare basalts and basaltic breccias that occur among Apollo and Luna samples [1], there are only 28 lunar meteorite stones that are either unbrecciated mare basalt or breccias dominated by large (>1 cm) clasts of mare basalt or gabbro [2]. When pairing is taken into consideration, these stones merely represent 11 meteorites [3]. Raman spectroscopy has proven to be robust in phase identification, quantification of phase proportions, characterizing structure and composition of solid solutions, distinguishing polymorphism, and extracting pressure records [e.g., 4-11]. Our work applied Raman spectroscopy to constrain the diverse mineralogy and pervasive shock metamorphism, and understand the petrogenetic and shock history of a young (crystallization age ~3.0 Ga, [12-14]) and Fe-rich (21.2 wt.% FeO, Mg<sup>\*</sup>=36.5, [12]) lunar mare basalt, Northwest Africa (NWA) 4734.

**Analytical Methods:** Raman spectroscopic measurements of NWA 4734 thick section were performed using the Renishaw inVia® Raman Microscope at Shandong University, Weihai, China and Washington University in St. Louis. The section was also examined via backscattered electron (BSE) imaging (Fig. 1) to understand petrogenetic relationships, and energy dispersive spectrometry (EDS) to identify Raman featureless phases. BSE and EDS analyses were performed by FEI SEM and Oxford X-Max EDS System at Shandong University, Weihai.

### Results and Discussion:

**Modal mineralogy and mineral chemistry.** We determined modal mineralogy of the NWA 4734 section by point-counting (n=376) Raman analyses. NWA 4734 comprises pyroxene (57.9%), plagioclase/maskelynite (28.8%) and olivine (3.7%), as well as mesostasis regions composed of Fe-rich pyroxene, K-feldspar, fayalite, silica polymorphs, Fe-metal/sulfide, phosphates, and Zr-bearing phases (Table 1). Mineral chemistries of pyroxene and olivine are calculated based on their Raman peak position shift [6, 8]. Pyroxenes in NWA 4734 exhibit bimodal extensive zoning (F<sub>S21-83</sub>W<sub>O10-40</sub>E<sub>N2-54</sub>), ranging from pigeonite to ferroaugite, and then extending through the “forbidden region” toward pyroxferroite (Fig. 2). Olivine occurs as two compositional clusters (Fig. 2, 3), phenocrysts with immediate Fo<sub>38-70</sub> or fayalitic patches (Fa<sub>73-97</sub>) in mesostasis.

Plagioclase has been partially (53.1%) transformed into maskelynite. Surviving plagioclase grains are also shocked to some degree, evidenced by broadened Raman peaks. Raman peak positions of these plagioclases are of the anorthite endmember and bytownite (An<sub>≥70</sub>, [7]). Accessory K-feldspar intergrown with Si-rich phases is observed in the mesostasis.

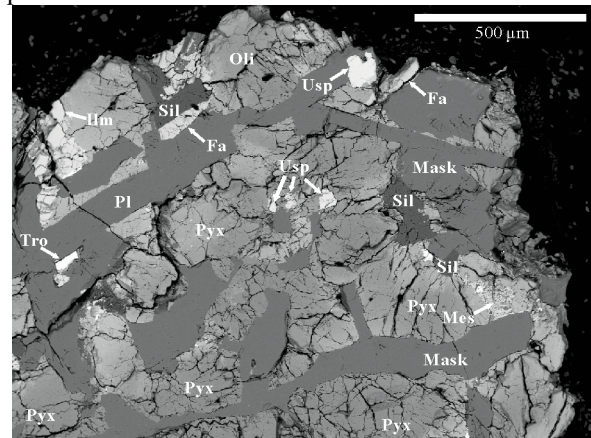


**Figure 1.** Backscattered electron (BSE) image of local area within NWA 4734 showing texture and phases.

Table 1. Modal mineralogy of NWA 4734 subsamples.

Reference	Raman	[12]	[14]
Pyroxene	57.9	58.1	58.0±2.5
Plag/Mask	28.8	25.6	30.6±3.4
Olivine	3.7	9.5	3.8±2.2
Ilmenite	1.5	2.9	2.2±1.1
Spinel	0.4	0.6	0.7±0.2
Silica	2.6	1.8	1.5±0.7
Fe-Metal/Sulfide	0.7	0.3	0.1±0.1
Phos&Zr-rich minerals	0.8	0.4	0.5±0.2
K-spar/Si-K Glass	1.0	1.5	0.3±0.1
Shock melt	2.6	na	2.3±1.4

Ilmenite occurs as elongate laths along phase boundaries or within mesostasis. Raman peak positions of ilmenite show that there is no obvious compositional variation deviating from the endmember FeTiO<sub>3</sub> [9]. Spinel within NWA 4734 consists of chromite and chromian ulvöspinel (the majority). Rutile and anatase (TiO<sub>2</sub>) polymorphs are observed within the mesostasis in close association with ilmenite and ulvöspinel.

Silica polymorphs include mainly shocked tridymite, but also quartz grains intergrown with K-feldspar. Coesite grains are observed within the silica glass along shock melt. Phosphates consist of apatite

and merrillite. The Raman spectrum of merrillite shows strong fluorescence background from the REE. Zr-bearing minerals are represented by baddeleyite, tranquillityite, and zirkelite.

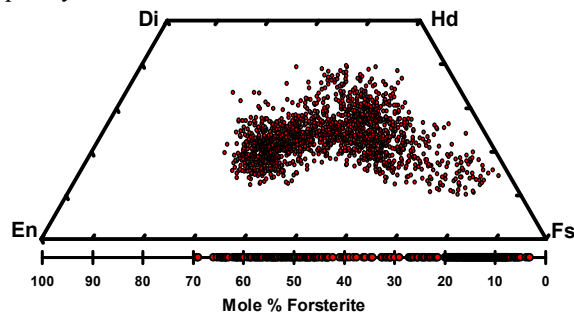


**Figure 2.** Quadrilateral pyroxene and olivine chemistries for NWA 4734 from Raman analyses.

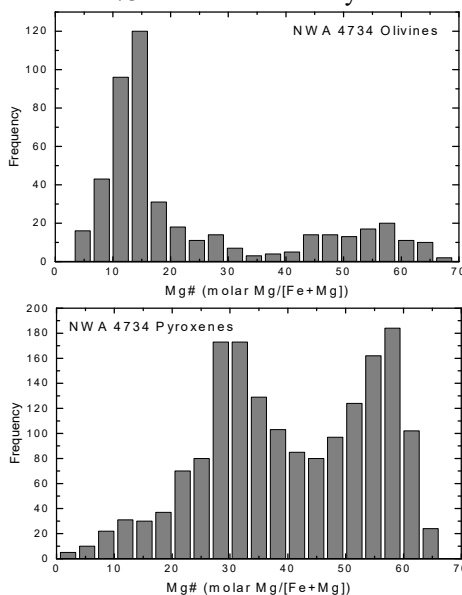


**Figure 3.** Bimodal Mg# frequency distributions of olivine (n=347) and pyroxene (n=1707) obtained by point-counting Raman experiments.

**Petrogenesis.** Based on petrography and mineral chemistry, we infer that NWA 4734 was derived from multi-stage crystallization. Coarse-grained olivine (with intermediate Fo values) and pyroxene (pigeonite cores) crystallized when the parental magma cooled down relatively slowly in the magma chamber or during its ascent through the lunar crust. Olivine phenocrysts stopped forming or resorbed when the pyroxene evolved to ferroaugite.

Eruption to the lunar surface led to more rapid cooling of the lava and pyroxene evolved to Fe-rich pyroxferroite. Fayalitic olivine occurred in the mesostasis regions and commonly served as the host to late stage mineral assemblages (e.g., Fe sulfide, silica, merrillite), possibly formed by immiscibility of silica-rich and residual iron-rich melts [15-16].

**Shock pressure.** Heavily fractured and disordered pyroxene and olivine phenocrysts, partly isotropic plagioclase, the existence of high pressure silica polymorphs, shock melt veins and pockets, and younger Ar-Ar age (sensitive to thermal events) than its crystallization age [17] indicate that NWA 4734 experienced extensive shock metamorphism after crystallization.

The intergrowth of silica polymorphs records continuous pressure-induced phase transitions, suggesting that the distribution of shock intensities is heterogeneous. Raman peak positions of quartz between  $\sim 461$ - $463$   $\text{cm}^{-1}$  indicate the shock pressure endured by the quartz was between 21.7-25.8 GPa [11].

Given that more calcic plagioclase requires lower shock pressure for maskelynitization [18], the remnant of anorthite or bytownite in NWA 4734 confines the shock pressure to lower than 25 GPa [19], which is consistent with the values recorded in quartz although high pressure silica polymorphs (stishovite and seifertite) have been reported in other studies [20-21].

**Acknowledgements:** This study is supported by the National Natural Science Foundation of China (No. 41473065), Natural Science Foundation of Shandong Province (JQ201511), the State Scholarship Fund (No. 201706220310), and the McDonnell Center for Space Sciences for a special financial support that enable the collaboration between the Department of Earth and Planetary Sciences at Washington University in St. Louis and School of Space Sciences and Physics at Shandong University, Weihai. We thank J. Y. Tan, W. B. Hsu and K. L. Wang for their help in sample preparation at PMO and SEM experiments at SDUW.

**References:** [1] Lucey P. et al. (2006) *RMG*, 60, 83-219. [2] <http://www.lpi.usra.edu/meteor/metbull.php>. [3] [http://meteorites.wustl.edu/lunar/moon\\_meteorite\\_s\\_list\\_alumina.htm](http://meteorites.wustl.edu/lunar/moon_meteorite_s_list_alumina.htm). [4] Wang A. et al. (1995) *JGR*, 100, 21189-21199. [5] Haskin L. A. et al. (1997) *JGR*, 102, 19293-19306. [6] Wang A. et al. (2001) *AM*, 86, 790-806. [7] Freeman J. J. et al. (2008) *CM*, 46, 1477-1500. [8] Kuebler K. E. et al. (2006) *GCA*, 70, 6201-6222. [9] Wang A. et al. (2004) *AM*, 89, 665-680. [10] Seddio S. M. et al. (2013) *LPS* 44, Abstract #2568. [11] McMillan P. F. et al. (1992) *PCM*, 19, 71-79. [12] Elardo S. M. et al. (2014) *Meteoritics & Planet. Sci.*, 49, 261-291. [13] Jambon A. (2009) *AMSM* 72, Abstract #5006. [14] Wang Y. (2012) *GCA*, 92, 329-344. [15] Roedder E. (1978) *GCA*, 42, 1597-1617. [16] Jolliff B. L. et al. (1999) *AM*, 84, 821-837. [17] Fernandes V. A. et al. (2009) *LPSC* 40, Abstract #1045. [18] Fritz J. et al. (2011) *LPSC* 42, Abstract #1196. [19] Rubin A. E. (2015) *Icarus*, 257, 221-229. [20] Chennaoui Aoudjehane H. and Jambon A. (2008) *AMSM* 71, Abstract #5058. [21] Miyahara M. (2013) *NC*, 4, 1737.